Vietnam Journal of Science and Technology ***60*** *(5) (2022) 869-881*

doi:10.15625/2525-2518/16172

BIMATERIAL INTERFACE CRACK ANALYSIS USING AN EXTENDED CONSECUTIVE-INTERPOLATION QUADRILATERAL ELEMENT

Thien Tich Truong[1, 2, *], Bang Kim Tran[1, 2], Vay Siu Lo[1, 2], Nha Thanh Nguyen[1, 2], Minh Ngoc Nguyen[3]

[1]*Department of Engineering Mechanics, Faculty of Applied Science, Ho Chi Minh City University of Technology (HCMUT), 268 Ly Thuong Kiet Str., Dist.10, Ho Chi Minh City, Viet Nam*

[2]*Vietnam National University Ho Chi Minh City, Linh Trung Ward, Thu Duc District, Ho Chi Minh City, Viet Nam*

[3]*Duy Tan Research Institute for Computational Engineering (DTRICE), Duy Tan University, 6 Tran Nhat Duat, District 1, Ho Chi Minh City, Viet Nam*

[*]Emails: *tttruong@hcmut.edu.vn*

Received: 17 June 2021; Accepted for publication: 31 October 2022

Abstract. A very important problem in the research of layer structures is the modelling of cracks on the material interface. Due to the complex physical and mechanical properties of this structure, the simulation of discontinuities such as cracks and material interface by traditional finite element methods requires a very fine mesh density. Furthermore, mesh smoothing requires a really large amount of computational resources. Therefore, an extended algorithm which does not require the remeshing technique was born to solve the crack problems. In this paper, the extended consecutive-interpolation finite element method (XCFEM) is employed to model the mix-mode interface cracks between two dissimilar isotropic materials. This will take advantage of the idea of the consecutive-interpolation finite element method (CFEM) and the enrichment functions of XFEM for discontinuous problems. The XCFEM using 4-node consecutive-interpolation quadrilateral element (XCQ4) provides continuity nodal gradient due to the concept of "consecutive-interpolation", so the stress and strain fields derived from XCQ4 is smoother than those obtained by the classical FEM element. The accuracy and effectiveness of the method are demonstrated via various numerical examples and compared with other researches.

Keywords: bimaterial interface crack, consecutive-interpolation procedure, extended consecutive-interpolation quadrilateral element.

Classification numbers: 5.4.3, 5.4.5, 5.4.6.

1. INTRODUCTION

Along with the development of industries, the complexity of materials is increasing in response to various requirements when materials are put into use. In particular, structures with

complex welds are used a lot in modern industry due to their scientific effectiveness. In welds, cracks are more likely to appear on the material interface, leading to the phenomenon of cracks that can penetrate the boundary between the two materials. Therefore, the analysis to predict the stress intensity factors (SIFs) of the interface crack in the bimaterial structure is really important.

For bimaterial interface cracks, Williams [1] laid the theoretical foundation, which was further developed by Rice and Sih [2]. Rice [3] clarified the meaning of the complex stress intensity factor, proposing a complex **K** for bimaterial interfacial cracks that can be reduced to the conventional definition (K_I, K_{II}) in the absence of any mismatch in material properties. In the case of a crack that runs along a bimaterial interface, the stresses are oscillatory in addition to singularity. Because the oscillatory singularity adds significant complexity to an element formulation, incorporating the radial dependence ($r^{i\varepsilon}$) of the crack-tip displacement field has not been attempted in the traditional finite element framework. Bimaterial interface cracks have already been studied through many numerical methods, for example, Nagashima [4], Sukumar [5] and Wang [6] used the extended finite element method (XFEM), Chen [7] employed the edge-based smoothed finite element method (ES-FEM), An [8] used the numerical manifold method, while the generalized finite difference method was employed by Jiang [9].

The conventional finite element method (FEM), however, produces the discontinuity of nodal gradient. To resolve this issue, Zheng *et al*. [10] developed a new concept of the "twice-interpolation" process acting on the interpolation functions in an enhanced triangular element for elastostatic problems. Then, Bui *et al*. [11] formulated a 4-node quadrilateral element for stress analysis of 2D elastic solids using the same manner. Furthermore, Bui *et al*. changed the term "twice-interpolation" to "consecutive-interpolation" in their work. As a result, the CQ4 (consecutive-interpolation 4-node quadrilateral element) was created [11]. Following that, Kang *et al*. [12] proposed the extended CQ4 (XCQ4) element based on the concept of CQ4 and XFEM.

In this study, the authors will investigate the behavior of cracks located on the material interface with the existing enrichment model for interface crack and develop it using the XCQ4 element. This will take advantage of the idea of the consecutive-interpolation finite element method (CFEM) and the enrichment functions of XFEM for discontinuous problems. The CFEM approximation functions will be extended by adding enrichment functions describing the crack discontinuities located on the material boundary. The validity of the study is examined through various numerical examples, demonstrating the accuracy of the approach.

2. METHODOLOGY

2.1. The consecutive-interpolation quadrilateral element (CQ4)

In the conventional FEM, the displacement of an arbitrary point $\mathbf{x} = (x, y)$ is approximated by the equation $u(\mathbf{x}) = \mathbf{N}(\mathbf{x})\mathbf{q}$, where $\mathbf{N}(\mathbf{x}) = \left[N_1(\mathbf{x})\ \ N_2(\mathbf{x})\ \ ...\ \ N_n(\mathbf{x})\right]$ is the vector containing shape functions and $\mathbf{q} = \left[u(\mathbf{x}_1)\ \ u(\mathbf{x}_2)\ \ ...\ \ u(\mathbf{x}_n)\right]^T$ is the vector of nodal values.

Defining $u^{[i]} = u(\mathbf{x}_i)$ as the displacement value of node *i* and $\mathbf{N}^{[i]} = \mathbf{N}(\mathbf{x}_i)$ as the vector of shape functions of node *i*, the average nodal displacement derivatives are defined as [10]

$$\bar{u}_{,x}^{[i]} = \sum_{e \in S_i} \omega_e u_{,x}^{[i][e]} = \sum_{e \in S_i} \left(\omega_e \mathbf{N}_{,x}^{[i][e]}\right)\mathbf{q} \tag{1}$$

and $\bar{\mathbf{N}}_{,x}^{[i]}$ are the average derivatives of $\mathbf{N}^{[i]}$, and computed as

$$\bar{\mathbf{N}}_{,x}^{[i]} = \sum_{e \in S_i} \left(\omega_e \mathbf{N}_{,x}^{[i][e]} \right) \tag{2}$$

where $u_{,x}^{[i][e]}$ and $\mathbf{N}_{,x}^{[i][e]}$ are the derivatives of $u^{[i]}$ and $\mathbf{N}^{[i]}$ calculated in element e, ω_e is a weight function dependent on element type, and for 2D element the weight function is computed as [11]

$$\omega_e = \frac{\Delta_e}{\sum_{e' \in S_i} \Delta_{e'}}, \quad e \in S_i \tag{3}$$

in which Δ_e is the area of the element e, and S_i are the support domains containing all the elements connected to node i as shown in Figure 1.

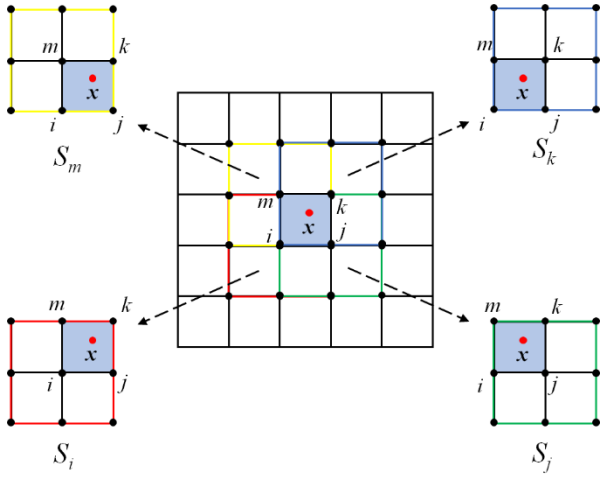

Figure 1. 2D consecutive-interpolation quadrilateral element and its support domains.

Figure 1 illustrates the support domains of the quadrilateral element in a finite element mesh. The support domains S_i, S_j, S_k and S_m consist of all the nearby elements of nodes *i*, *j*, *k* and *m*, respectively. It is clearly observed that the supporting nodes for the point of interest **x** contain all the nodes in the support domains.

The discontinuity of the nodal gradients causes the discontinuous stress in the standard FEM. Therefore, according to [10], the average derivatives obtained by the conventional FEM are considered as interpolation conditions. In the consecutive-interpolation procedure, both the nodal values $u^{[i]}$ and the averaged nodal derivatives $\bar{u}_{,x}^{[i]}$ are selected as interpolation conditions. The approximation functions can be stated as follows [11]

$$\hat{u}(\mathbf{x}) = \sum_{i=1}^{n} \left(\phi_i u^{[i]} + \phi_{ix} \bar{u}_{,x}^{[i]} + \phi_{iy} \bar{u}_{,y}^{[i]} \right) = \sum_{i=1}^{n} \left(\phi_i \mathbf{N}^{[i]} + \phi_{ix} \bar{\mathbf{N}}_{,x}^{[i]} + \phi_{iy} \bar{\mathbf{N}}_{,y}^{[i]} \right) \mathbf{q} \tag{4}$$

and the shape functions are expressed as

$$\hat{\mathbf{N}} = \sum_{i=1}^{n} \left(\phi_i \mathbf{N}^{[i]} + \phi_{ix} \bar{\mathbf{N}}_{,x}^{[i]} + \phi_{iy} \bar{\mathbf{N}}_{,y}^{[i]} \right) \tag{5}$$

where $\phi_i, \phi_{ix}, \phi_{iy}$ are field functions dependent on the element type. The field functions $\phi_i, \phi_{ix}, \phi_{iy}$ must satisfy the following conditions [10].

$$\begin{aligned} &\phi_i(\mathbf{x}_l) = \delta_{il}, \quad \phi_{i,x}(\mathbf{x}_l) = 0, \quad \phi_{i,\mathrm{y}}(\mathbf{x}_l) = 0 \\ &\phi_{ix}(\mathbf{x}_l) = 0, \quad \phi_{ix,x}(\mathbf{x}_l) = \delta_{il}, \quad \phi_{ix,\mathrm{y}}(\mathbf{x}_l) = 0 \\ &\phi_{iy}(\mathbf{x}_l) = 0, \quad \phi_{iy,x}(\mathbf{x}_l) = 0, \quad \phi_{iy,\mathrm{y}}(\mathbf{x}_l) = \delta_{il} \end{aligned} \tag{6}$$

Where *l* can be any one of the indices *i*, *j*, *k* and *m* (quadrilateral element), and

$$\delta_{ij} = \begin{cases} 1 & if\ i = j \\ 0 & if\ i \neq j \end{cases} \tag{7}$$

For 4-node quadrilateral element, according to [11], the field functions are defined as

$$\begin{aligned} \phi_i &= L_i + L_i^2 L_j + L_i^2 L_k + L_i^2 L_m - L_i L_j^2 - L_i L_k^2 - L_i L_m^2 \\ \phi_{ix} &= -(x_i - x_j)(L_i^2 L_j + pL_i L_j L_k + pL_i L_j L_m) \\ &\quad -(x_i - x_k)(L_i^2 L_k + pL_i L_k L_m + pL_i L_k L_j) \\ &\quad -(x_i - x_m)(L_i^2 L_m + pL_i L_m L_j + pL_i L_m L_k) \\ \phi_{iy} &= -(\mathrm{y}_i - y_j)(L_i^2 L_j + pL_i L_j L_k + pL_i L_j L_m) \\ &\quad -(\mathrm{y}_i - y_k)(L_i^2 L_k + pL_i L_k L_m + pL_i L_k L_j) \\ &\quad -(\mathrm{y}_i - y_m)(L_i^2 L_m + pL_i L_m L_j + pL_i L_m L_k) \end{aligned} \tag{8}$$

in which L_i, L_j, L_k, L_m are the Lagrange basis functions.

In Equation (8), $p = 1/2$ and the $\phi_j, \phi_{jx}, \phi_{jy}$; $\phi_k, \phi_{kx}, \phi_{ky}$ and $\phi_m, \phi_{mx}, \phi_{my}$ functions can be calculated in the same manner by a cyclic permutation of indices *i*, *j*, *k* and *m*.

After substituting the field function into Equation (4), the approximation equation can be expressed as

$$\hat{u}(\mathbf{x}) = \sum_{l=1}^{n_s} \hat{N}_l(\mathbf{x}) q_l = \hat{\mathbf{N}}(\mathbf{x})\mathbf{q} \tag{9}$$

where n_s is the number of supporting nodes. The shape function of node *l* is computed as the following equation [12]

$$\begin{aligned} \hat{N}_l = &\underbrace{\phi_i N_l^{[i]} + \phi_{ix} \bar{N}_{l,x}^{[i]} + \phi_{iy} \bar{N}_{l,y}^{[i]}}_{node\ i} + \underbrace{\phi_j N_l^{[j]} + \phi_{jx} \bar{N}_{l,x}^{[j]} + \phi_{jy} \bar{N}_{l,y}^{[j]}}_{node\ j} \\ &+ \underbrace{\phi_k N_l^{[k]} + \phi_{kx} \bar{N}_{l,x}^{[k]} + \phi_{ky} \bar{N}_{l,y}^{[k]}}_{node\ k} + \underbrace{\phi_m N_l^{[m]} + \phi_{mx} \bar{N}_{l,x}^{[m]} + \phi_{my} \bar{N}_{l,y}^{[m]}}_{node\ m} \end{aligned} \tag{10}$$

2.2. The extended consecutive-interpolation quadrilateral element (XCQ4)

According to [10], the nodal derivatives obtained by the consecutive-interpolation procedure are continuous. However, there are cases where C^0-continuity at node is required, for

instances on material interfaces or boundaries, such as bimaterial interface and crack. In such cases, following the work of [12], it is essential to modify Equation (2), such that the average shape functions gradient in Equation (2) is replaced by the nodal gradient

$$\bar{N}_{I,x}^{[i]} = N_{I,x}^{[i][e]} \tag{11}$$

Similar to the XFEM procedure, the XCQ4 adds some enriched treatments for discontinuity problems. It is achieved by handling appropriate enrichment functions, the displacement field near the crack is enhanced by adding a discontinuous Heaviside function across the crack faces and the asymptotic branch functions (tip enrichment) around the crack tip. By including enrichment functions, the displacement is now computed as [12].

$$\begin{aligned}\mathbf{u}^h(\mathbf{x}) = &\sum_{i\in N} N_i(\mathbf{x})\mathbf{u}_i + \sum_{j\in N^{split}} N_j(\mathbf{x})\Big[H(\mathbf{x}) - H(\mathbf{x}_j)\Big]\mathbf{a}_j \\ &+ \sum_{l\in N^{tip}} N_l(\mathbf{x})\sum_{\alpha}\Big[F_\alpha(\mathbf{x}) - F_\alpha(\mathbf{x}_l)\Big]\mathbf{c}_l\end{aligned} \tag{12}$$

where $H(\mathbf{x})$ is the Heaviside function of point $\mathbf{x}$ and $H(\mathbf{x}_j)$ is the Heaviside function of node j, the Heaviside function is defined as

$$H\big(f(\mathbf{x})\big) = \begin{cases} 1 & if\ \ f(\mathbf{x}) > 0 \\ -1 & if\ \ f(\mathbf{x}) < 0 \end{cases} \tag{13}$$

$f(\mathbf{x})$ is the sign distance function.

The tip enrichment function $F_\alpha(\mathbf{x})$ will be detailed in the next section for the bimaterial interface crack. Equation (13) includes three sets of node. The first set N contains all nodes in the computational domain. The second set N^{split} is the set containing the nodes in the elements split by the crack. And N^{tip} is the set containing the nodes in the element that contains the crack tip.

In the discrete equation of finite element analysis, one must remember that the stiffness matrix is computed as

$$\mathbf{K} = \int_A \mathbf{B}^T\mathbf{D}\mathbf{B}dA \tag{14}$$

where $\mathbf{D}$ is the material matrix, $\mathbf{B}$ is the matrix containing the derivatives of the shape functions. At node I, $\mathbf{B}_I$ includes three components.

$$\mathbf{B}_I = \begin{bmatrix}\mathbf{B}_I^{standard} & \mathbf{B}_I^{split,enrich} & \mathbf{B}_I^{tip,enrich,\alpha}\end{bmatrix} \tag{15}$$

The $\mathbf{B}_I^{standard}$ matrix for all nodes is computed as

$$\mathbf{B}_I^{standard} = \begin{bmatrix} N_{I,x} & 0 \\ 0 & N_{I,y} \\ N_{I,y} & N_{I,x} \end{bmatrix} \tag{16}$$

The $\mathbf{B}_I^{split,enrich}$ matrix for the split nodes is calculated as the following equation

$$\mathbf{B}_I^{split,enrich} = \begin{bmatrix} N_{I,x}\big(H(\mathbf{x}) - H(\mathbf{x}_I)\big) & 0 \\ 0 & N_{I,y}\big(H(\mathbf{x}) - H(\mathbf{x}_I)\big) \\ N_{I,y}\big(H(\mathbf{x}) - H(\mathbf{x}_I)\big) & N_{I,x}\big(H(\mathbf{x}) - H(\mathbf{x}_I)\big) \end{bmatrix} \tag{17}$$

and for the tip nodes, the $\mathbf{B}_I^{tip,enrich,\alpha}$ matrix is expressed as

$$\mathbf{B}_I^{tip,enrich,\alpha} = \begin{bmatrix} \left[N_I\left(F_\alpha(\mathbf{x}) - F_\alpha(\mathbf{x}_I)\right)\right]_{,x} & 0 \\ 0 & \left[N_I\left(F_\alpha(\mathbf{x}) - F_\alpha(\mathbf{x}_I)\right)\right]_{,\mathrm{y}} \\ \left[N_I\left(F_\alpha(\mathbf{x}) - F_\alpha(\mathbf{x}_I)\right)\right]_{,\mathrm{y}} & \left[N_I\left(F_\alpha(\mathbf{x}) - F_\alpha(\mathbf{x}_I)\right)\right]_{,x} \end{bmatrix} \tag{18}$$

2.3. Bimaterial interface crack

Considering a bimaterial plate with an interface crack as shown in Figure 2. Using the XCQ4 approximation, the displacement field can be written as [13].

$$\begin{aligned} \mathbf{u}^h(\mathbf{x}) = &\sum_{i\in N} N_i(\mathbf{x})\mathbf{u}_i + \sum_{j\in N^{split}} N_j(\mathbf{x})\left[H(\mathbf{x}) - H(\mathbf{x}_j)\right]\mathbf{a}_j \\ &+ \sum_{k\in N^{\text{interface}}} N_k(\mathbf{x})\chi_k(\mathbf{x})\mathbf{b}_k + \sum_{l\in N^{tip}} N_l(\mathbf{x})\sum_{\alpha=1}^{12}\left[F_\alpha(\mathbf{x}) - F_\alpha(\mathbf{x}_l)\right]\mathbf{c}_l \end{aligned} \tag{19}$$

where $N^{\text{interface}}$ is the set containing the nodes in the elements split by the bimaterial interface. Figure 2 illustrates three sets of enriched nodes in the bimaterial interface crack problem.

To model the interface crack, the tip enrichment functions $F_\alpha(\mathbf{x})$ for a bimaterial interfacial crack are introduced as [5].

$$\begin{aligned} \left[F_\alpha(\mathbf{x}), \alpha = 1-12\right] = \Big\{ &\sqrt{r}\cos(\varepsilon\log r)e^{-\varepsilon\theta}\sin\frac{\theta}{2}, \sqrt{r}\cos(\varepsilon\log r)e^{-\varepsilon\theta}\cos\frac{\theta}{2}, \\ &\sqrt{r}\cos(\varepsilon\log r)e^{\varepsilon\theta}\sin\frac{\theta}{2}, \sqrt{r}\cos(\varepsilon\log r)e^{\varepsilon\theta}\cos\frac{\theta}{2}, \\ &\sqrt{r}\cos(\varepsilon\log r)e^{\varepsilon\theta}\sin\frac{\theta}{2}\sin\theta, \sqrt{r}\cos(\varepsilon\log r)e^{\varepsilon\theta}\cos\frac{\theta}{2}\sin\theta, \\ &\sqrt{r}\sin(\varepsilon\log r)e^{-\varepsilon\theta}\sin\frac{\theta}{2}, \sqrt{r}\sin(\varepsilon\log r)e^{-\varepsilon\theta}\cos\frac{\theta}{2}, \\ &\sqrt{r}\sin(\varepsilon\log r)e^{\varepsilon\theta}\sin\frac{\theta}{2}, \sqrt{r}\sin(\varepsilon\log r)e^{\varepsilon\theta}\cos\frac{\theta}{2}, \\ &\sqrt{r}\sin(\varepsilon\log r)e^{\varepsilon\theta}\sin\frac{\theta}{2}\sin\theta, \sqrt{r}\sin(\varepsilon\log r)e^{\varepsilon\theta}\cos\frac{\theta}{2}\sin\theta \Big\} \end{aligned} \tag{20}$$

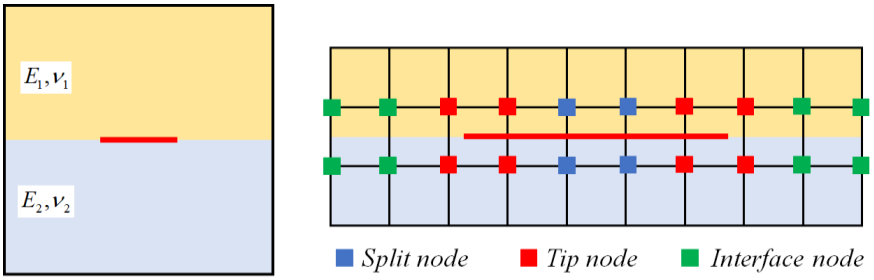

Figure 2. Bimaterial interface crack and enriched nodes.

where r and θ are polar coordinates in the local crack tip coordinate system, ε is the index of oscillation and defined as

$$\varepsilon = \frac{1}{2\pi}\log\left(\frac{1-\beta}{1+\beta}\right) \tag{21}$$

in which β is the second Dundurs parameter for isotropic materials [14].

$$\beta = \frac{\mu_1(\kappa_2 - 1) - \mu_2(\kappa_1 - 1)}{\mu_1(\kappa_2 + 1) + \mu_2(\kappa_1 + 1)} \tag{22}$$

The parameters in Equation (22) are defined as

$$\mu_i = \frac{E_i}{2(1+\nu_i)},\ (i=1,2) \qquad \kappa_i = \begin{cases} (3-\nu_i)/(1+\nu_i) & \text{(Plane stress)} \\ 3-4\nu_i & \text{(Plane strain)} \end{cases} (i=1,2) \tag{23}$$

It is observed that a new enrichment function is added to Equation (19) to model the discontinuity at the material interface. $\chi_k(\mathbf{x})$ is the weak discontinuous enrichment function [15] defined in terms of the signed distance function $f(\mathbf{x})$

$$\chi_k(\mathbf{x}) = \left|f(\mathbf{x})\right| - \left|f(\mathbf{x}_k)\right| \tag{24}$$

To determine the mixed-mode stress intensity factors (SIFs) in 2D interfacial fracture computations, the domain form of the interaction integral is a well-established technique [16, 17].

$$I = -\int_A \left(\sigma_{ik}\varepsilon_{ik}^{aux}\delta_{1j} - \sigma_{ij}u_{i,x}^{aux} - \sigma_{ij}^{aux}u_{i,x}\right)q_{,j}\,dA \tag{25}$$

where u_i^{aux}, ε_{ij}^{aux}, σ_{ij}^{aux} are the auxiliary displacement, strain and stress fields, respectively. The relationship between the interaction integral and the SIFs [18].

$$I = \frac{2}{E^*\cosh^2(\pi\varepsilon)}\left[K_1K_1^{aux} + K_2K_2^{aux}\right] \tag{26}$$

The stress intensity factor K_1 can be obtained by selecting $K_1^{aux} = 1$ and $K_2^{aux} = 0$, then computing the interaction integral $I = I_1$ in Equation (25) and using Equation (26) to acquire the value of K_1. K_2 can be derived in the same manner. E^* is determined as the following.

$$\frac{2}{E^*} = \frac{1}{\bar{E}_1} + \frac{1}{\bar{E}_2}, \quad \bar{E}_i = \begin{cases} E_i & (\textit{plane stress}) \\ \dfrac{E_i}{1-\nu_i^2} & (\textit{plane strain}) \end{cases} (i=1,2) \tag{27}$$

where E is Young's modulus and ν is Poisson ratio.

The auxiliary field in Equation (25) is given by [19].

$$u_i = \begin{cases} \dfrac{1}{4\mu_1\cosh(\pi\varepsilon)}\sqrt{\dfrac{r}{2\pi}}\,f_i(r,\theta,\varepsilon,\kappa_1) & (\textit{upper}-\textit{half plane}) \\ \dfrac{1}{4\mu_2\cosh(\pi\varepsilon)}\sqrt{\dfrac{r}{2\pi}}\,f_i(r,\theta,\varepsilon,\kappa_2) & (\textit{lower}-\textit{half plane}) \end{cases} (i=1,2) \tag{28}$$

To extract K_1, the functions f_1 and f_2 are

$$f_1 = D + 2\delta \sin\theta \sin\varphi, \quad f_2 = -C - 2\delta \sin\theta \cos\varphi \tag{29}$$

meanwhile to compute K_2, the functions f_1 and f_2 are expressed as

$$f_1 = -C + 2\delta \sin\theta \cos\varphi, \quad f_2 = -D + 2\delta \sin\theta \sin\varphi \tag{30}$$

In the above equations, δ, φ, C and D are given by

$$\delta = \begin{cases} e^{-(\pi-\theta)\varepsilon} & (upper-half\ \ plane) \\ e^{(\pi+\theta)\varepsilon} & (lower-half\ \ plane) \end{cases} \tag{31}$$

$$\varphi = \varepsilon \log r + \frac{\theta}{2} \tag{32}$$

$$C = B'\gamma \cos\frac{\theta}{2} - B\gamma' \sin\frac{\theta}{2}, \quad D = B\gamma \cos\frac{\theta}{2} + B'\gamma' \sin\frac{\theta}{2} \tag{33}$$

$$B = \frac{0.5\cos(\varepsilon \log r) + \varepsilon \sin(\varepsilon \log r)}{0.25 + \varepsilon^2}, \quad B' = \frac{0.5\sin(\varepsilon \log r) - \varepsilon \cos(\varepsilon \log r)}{0.25 + \varepsilon^2} \tag{34}$$

$$\gamma = \kappa\delta - \frac{1}{\delta}, \quad \gamma' = \kappa\delta + \frac{1}{\delta}, \quad \kappa = \begin{cases} \kappa_1 & (upper-half\ \ plane) \\ \kappa_2 & (lower-half\ \ plane) \end{cases} \tag{35}$$

The displacement gradients of the auxiliary fields $u_{i,x}^{aux}$ can be found in [5].

3. RESULTS AND DISCUSSION

3.1. Center-crack in an infinite bimaterial plate

The first example to be considered is the problem of an interfacial crack located between two dissimilar elastic semi-infinite planes. The analytical solution to this problem under remote traction $\mathbf{t} = \sigma_{yy}^{\infty} + i\tau_{xy}^{\infty}$ was proposed by Rice and Sih [2]. The solution for K_1 and K_2 at the right crack tip is [3]:

$$\mathbf{K} = K_1 + iK_2 = \left(\sigma_{yy}^{\infty} + i\tau_{xy}^{\infty}\right)(1 + 2i\varepsilon)\sqrt{\pi a}(2a)^{-i\varepsilon} \tag{36}$$

The case of pure tension remote loading is investigated. In the numerical model, a large square plate containing a small center crack is considered (see Figure 3). The factor K_0 is used to normalize the stress intensity factors and computed as $K_0 = \sigma_{yy}^{\infty}\sqrt{\pi a}$, where 2*a* is the crack length.

Figure 3 shows the geometry of the cracked plate, the parameters chosen for this analysis are *W* = 30 *m* and *a* = 1 *m*. The material constants used in the numerical computations are: $E_1/E_2 = 22$, $E_2 = 10^3\ Pa$, $\nu_1 = 0.2571$ and $\nu_2 = 0.3$ [19], and plane strain conditions are assumed. The exact solution from Equation (36) is

$$\frac{K_1}{K_0} = 1.008, \quad \frac{K_2}{K_0} = -0.1097 \tag{37}$$

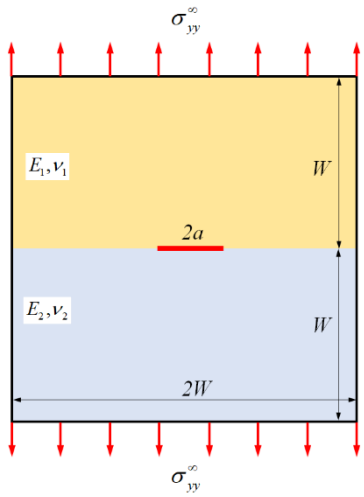

Figure 3. Center crack under remote tension.

A structural mesh is employed in this example, and the model is discretized into a set of 120×120 nodes due to the small crack compared to the size of the plate. Table 1 shows the normalized SIFs obtained in this study compared to other methods. The relative error of the result is computed as

$$\%error = \frac{\left|\left(K_1/K_0\right)_{numerical} - \left(K_1/K_0\right)_{analytical}\right|}{\left(K_1/K_0\right)_{analytical}} \times 100 \tag{38}$$

It is seen that the XCQ4 agrees well with the analytical solution and other numerical methods. With the same mesh size as mentioned above, the XFEM result obtained in this study (the row below XQC4 in Table 1) is more in error than the XCQ4 result. Particularly, the errors of XFEM are 2.69 % and 3.63 %, while the errors of XCQ4 are only 0.11 % and 1.68 %. Furthermore, the normalized K_2 is smaller compared to the normalized K_1, it is reasonable because the opening mode loading is applied at the top and bottom edges of the plate.

Table 1. The normalized SIFs in different methods.

Method	K_1/K_0 (% error)	K_2/K_0 (% error)
XCQ4	0.9982 (0.11)	-0.1078 (1.68)
XFEM	0.9808 (2.69)	-0.1057 (3.63)
XFEM [5]	1.0090 (0.10)	-0.1110 (1.19)
ES-FEM [7]	1.0041 (0.40)	-0.1104 (0.60)

To investigate the performance on interface fractures for various material property pairings, the ratio E_1/E_2 is varied from 2 to 1000. Table 2 shows the normalized K_1 values for the different methods, where the normalized K_1 tends to rise when the E_1/E_2 ratio increases. It is observed that the results are also accurate compared to other available solutions, demonstrating the usefulness of XCQ4 for bimaterial interface cracks.

Table 2. The normalized K_1 in material mismatch study.

E_1/E_2	XCQ4 K_1/K_0 (% error)	XFEM [5] K_1/K_0 (% error)	ES-FEM [7] K_1/K_0 (% error)	Analytical [5, 6] K_1/K_0
2	0.9673 (3.33)	1.002 (0.1)	0.9995 (0.12)	1.0007
4	0.9753 (2.76)	1.004 (0.1)	1.0016 (0.14)	1.0030
8	0.9828 (2.26)	1.007 (0.2)	1.0039 (0.17)	1.0056
40	0.9987 (1.01)	1.010 (0.1)	1.0072 (0.17)	1.0089
100	1.0042 (0.53)	1.010 (0.0)	1.0081 (0.14)	1.0096
1000	1.0082 (0.18)	1.010 (0.0)	1.0089 (0.11)	1.0100

3.2. Edge crack in a rectangular bimaterial plate

In this example, a rectangular with an edge crack on the material interface is investigated. The dimension of the plate is W = 1 m as shown in Figure 4, various crack lengths a are considered in this analysis. The material constants used in the numerical computations are: $E_1 = 10^3\ Pa$, $E_2/E_1 = 22$, $\nu_2 = 0.2571$ and $\nu_1 = 0.3$, and plane strain conditions are assumed. The bottom edge of the plate is fixed in x and y directions, the top edge is subjected to the uniform pressure $\sigma = 10^3\ Pa$. The discrete model of this problem consists of 50×100 nodes. In this study, for the sake of brevity, only a fine mesh is used. The convergence study of XCQ4 element with respect to mesh density can be found in [12].

Figure 5 shows the variation of the normalized stress intensity factors corresponding to the *a/W* ratios. From this figure, an upward trend in the normalized K_1 is observed as the *a/W* ratio increases. It also indicates that the results obtained from XCQ4 and XFEM are the same.

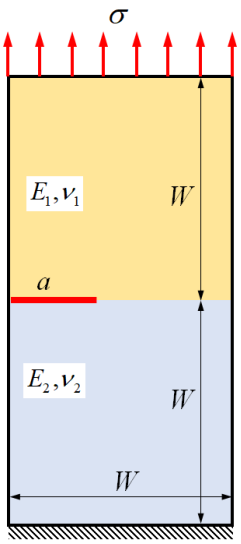

Figure 4. Geometry, load and boundary conditions in an edge crack plate.

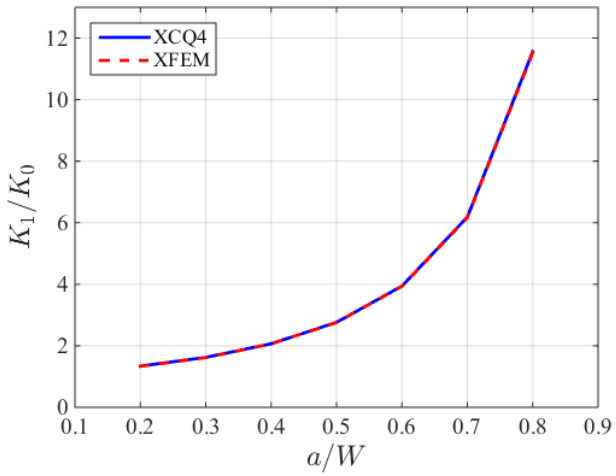

Figure 5. The variation of normalized K_1.

Figure 6 illustrates the von-Mises stress obtained in XCQ4 and XFEM when the ratio of crack length to plate length a/W = 0.5. It is clearly observed from this figure that the XCFEM using XCQ4 element can achieve a smoother stress at the crack tip than the one yielded by XFEM.

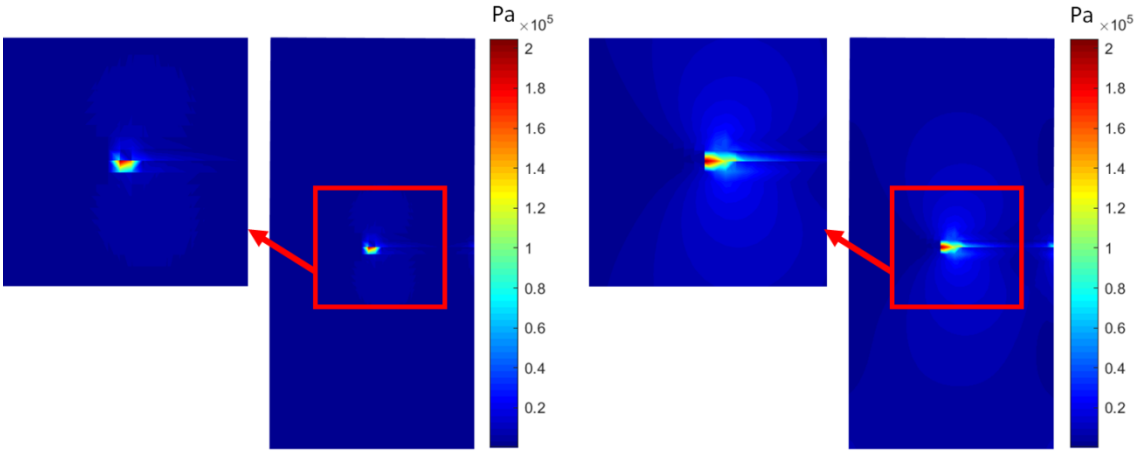

Figure 6. von-Mises stress in the case of a/W = 0.5. Left: XFEM result. Right: XCQ4 result.

4. CONCLUSIONS

In this study, the XCQ4 element is employed to evaluate the stress intensity factors of the bimaterial interface crack. With existing XFEM codes, it is effortless to implement the XCQ4 element. At the crack and material interface, however, the C^0-continuity at node is required to give an accurate XCQ4 result. In the numerical example, the result obtained from XCQ4 shows good agreement with the analytical solution and other numerical methods. The stress field near the crack tip derived from XCQ4 is smoother than that obtained by XFEM. This is a promising

method for the analysis of non-smoothed interface cracks due to the fact that the XCQ4 element provides not only better numerical solutions, but also smoother stress distributions at the crack tip, which the ordinary element cannot easily achieve.

Acknowledgements. This research is funded by Ho Chi Minh City University of Technology – VNU-HCM, under grant number To-KHUD-2020-11. We acknowledge the support of time and facilities from Ho Chi Minh City University of Technology (HCMUT), VNU-HCM for this study.

CRediT authorship contribution statement. Thien Tich Truong: Supervisor, Funding acquisition, Methodology. Bang Kim Tran: Methodology, Investigation. Vay Siu Lo: Gathering data, Manuscript editor. Nha Thanh Nguyen and Minh Ngoc Nguyen: Checking the results, Manuscript review.

Declaration of competing interest. The authors declare that they have no known competing financial interests or personal relationships that could have appeared to influence the work reported in this paper.

REFERENCES

1. Williams M. L. - The stress around a fault or crack in dissimilar media, Bulletin of the Seismology Society of America **49** (1959) 199-204.

   https://doi.org/10.1785/BSSA0490020199

2. Rice J. R. and Sih G. C. - Plane problems of cracks in dissimilar media, J. Appl. Mech. **32** (1965) 418-423. https://doi.org/10.1115/1.3625816

3. Rice J. R. - Elastic fracture mechanics concepts for interfacial cracks, J. Appl. Mech. **55** (1988) 98-103. https://doi.org/10.1115/1.3173668

4. Nagashima T., Omoto Y., and Tani S. - Stress intensity factor analysis of interface cracks using X-FEM, Int. J. Numer. Mech. Eng. **28** (2003) 1151-1173. https://doi.org/ 10.1002/nme.604

5. Sukumar N., Huang Z. Y., Prévost J. H., and Suo Z. - Partition of unity enrichment for bimaterial interface cracks, Int. J. Numer. Mech. Eng. **59** (2004) 1075-1102. https://doi.org/10.1002/nme.902

6. Wang Y. and Waisman H. - Material-dependent crack-tip enrichment functions in XFEM for modeling interfacial cracks in bimaterials, Int. J. Numer. Mech. Eng. **112** (2017) 1495-1518. https://doi.org/10.1002/nme.5566

7. Chen L., Liu G. R., Nourbakhsh-Nia N. and Zeng K. - A singular edge-based smoothed finite element method (ES-FEM) for bimaterial interface cracks, Comput. Mech. **45** (2010) 109-125. https://doi.org/10.1007/s00466-009-0422-3

8. An X. M., Zhao Z. Y., Zhang H. H., and He L. - Modeling bimaterial interface cracks using the numerical manifold method, Eng. Anal. Bound. Elem. **37** (2013) 464-474. https://doi.org/10.1016/j.enganabound.2012.11.014

9. Jiang S., Gu Y., Fan C. M., and Qu W. - Fracture mechanics analysis of bimaterial interface cracks using the generalized finite difference method, Theor. Appl. Fract. Mec. **113** (2021) 102942. https://doi.org/10.1016/j.tafmec.2021.102942

10. Zheng C., Wu S. C., Tang X. H., and Zhang J. H. - A novel twice-interpolation finite element method for solid mechanics problems, Acta Mech. Sin. **26** (2010) 265-278. https://doi.org/10.1007/s10409-009-0265-3

11. Bui T. Q., Vo D. Q., Zhang C., and Nguyen D. D. - A consecutive-interpolation quadrilateral element (CQ4): Formulation and applications, Finite Elem. Anal. Des. **84** (2014) 14-31. https://doi.org/10.1016/j.finel.2014.02.004
12. Kang Z., Bui T. Q., Nguyen D. D., Saitoh T., and Hirose S. - An extended consecutive-interpolation quadrilateral element (XCQ4) applied to linear elastic fracture mechanics, Acta Mech. **226** (2015) 3991-4015. https://doi.org/10.1007/s00707-015-1451-y
13. Mohammadi S. - XFEM fracture analysis of composites, John Wiley & Sons, 2012. https://doi.org/10.1002/9781118443378
14. Dundurs J. - Edge-bonded dissimilar orthogonal elastic wedges, J. Appl. Mech. **36** (1969) 650-652. https://doi.org/10.1115/1.3564739
15. Bordas S. and Legay A. - X-FEM Mini-Course, EPFL, Lausanne, 2005.
16. Shih C. F. and Asaro R. J. - Elastic-plastic analysis of cracks on bimaterial interfaces: Part I small scale yielding, J. Appl. Mech. **55** (1988) 299-316. https://doi.org/10.1115/1.3173676
17. Nahta R. and Moran B. - Domain integrals for axisymmetric interface crack problems, Int. J. Solids Struct. **30** (1993) 2027-2040. https://doi.org/10.1016/0020-7683(93)90049-D
18. Yau J. F., Wang S. S., and Corten H. T. - A mixed-mode crack analysis of isotropic solids using conservation laws of elasticity, J. Appl. Mech. **47** (1980) 335-341. https://doi.org/10.1115/1.3153665
19. Matos P. P. L., McMeeking R. M., Charalambides P. G., and Drory M. D. - A method for calculating stress intensities in bimaterial fracture, Int. J. Fract. **40** (1989) 235-254. https://doi.org/10.1007/BF00963659